JACS
JOURNAL OF THE AMERICAN CHEMICAL SOCIETY

ARTICLE

pubs.acs.org/JACS

Supramolecular Bola-Like Ferroelectric: 4-Methoxyanilinium Tetrafluoroborate-18-crown-6

Da-Wei Fu,[†] Wen Zhang,*[,†] Hong-Ling Cai,[†] Yi Zhang,[†] Jia-Zhen Ge,[†] Ren-Gen Xiong,*[,†] and Songping D. Huang[‡]

[†]Ordered Matter Science Research Center, Southeast University, Nanjing 211189, China

[‡]Department of Chemistry, Kent State University, Kent, Ohio 44240, United States

Supporting Information

ABSTRACT: Molecular motion is one of the structural foundations for the development of functional molecular materials such as artificial motors and molecular ferroelectrics. Herein, we show that pendulum-like motion of the terminal group of a molecule causes a ferroelectric phase transition. Complex 4-methoxyanilinium tetrafluoroborate-18-crown-6 ($[C_7H_{10}NO$-(18-crown-6)$]^+[BF_4]^-$, **1**) shows a second-order ferroelectric phase transition at 127 K, together with an abrupt dielectric anomaly, Debye-type relaxation behavior, and the symmetry breaking confirmed by temperature dependence of second harmonic generation effect. The origin of the polarization is due to the order−disorder transition of the pendulum-like motions of the terminal *para*-methyl group of the 4-methoxyanilinium guest cation; that is, the freezing of pendulum motion at low temperature forces significant orientational motions of the guest molecules and thus induces the formation of the ferroelectric phase. The supramolecular bola-like ferroelectric is distinct from the precedent ferroelectrics and will open a new avenue for the design of polar functional materials.

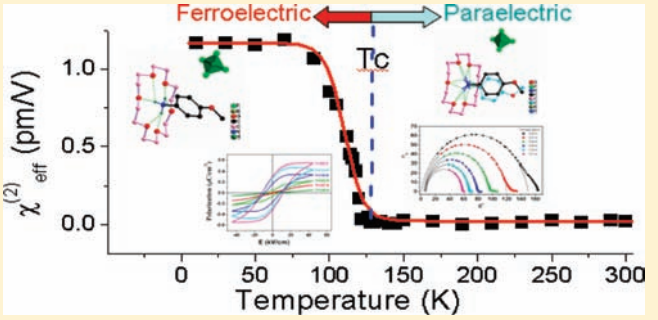

1. INTRODUCTION

Ferroelectric materials that exhibit reversible electric polarization in response to an external electric field have found many applications such as in nonvolatile memory storage, electronics, and optics.[1,2] Molecular rotation motion used as molecular rotors and gyroscopes has recently attracted much attention due in part to the development of artificial molecular motors or potential molecular dielectric rotors.[3−11] Molecular random rotary motion, for example, the 180° flip−flop motion of a rotatory unit, has proved to cause a rotation of the local structure to result in the formation of rotor phase transition from the high-temperature disordered state to the low-temperature ordered state. Recently, Akutagawa et al. pioneered to use such a transition to control molecular rotators in the design of ferroelectric molecular materials. As a polarization rotation unit, *m*-fluoroanilinium forms a hydrogen-bonding assembly with dibenzo[18]crown-6 with $[Ni(dmit)_2]^-$ counteranion ($dmit^{2-}$ = 2-thioxo-1,3-dithiole-4,5-dithiolate).[7] The supramolecular rotator *m*-fluoroanilinium exhibits dipolar rotation by application of an electric field, and the dielectric anomaly at about 348 K reveals a possible ferroelectric behavior.

The protonated R−NH_3^+ cation (R = aryl ring) is easily anchored in the cavity of 18-crown-6, which is a good molecular stator or pendulator in molecular machine design. However, as a great challenge, utilization of the R group as a molecular rotor or pendulum unit to create a detectable polar structural phase transition still remains unexplored. In the exploration of new types of molecular-based ferroelectrics,[12−17] the difficulties include that the ferroelectrics should meet with reversible structural phase transitions between paraelectric (adopting possible 32 point groups) and ferroelectric phases (adopting one of 10 polar point groups: C_1, C_2, C_3, C_4, C_6, C_s, C_{2v}, C_{3v}, C_{4v}, and C_{6v}), and there should be apparent dielectric anomaly or domain wall motion together with perfect standard dielectric hysteresis loop. Herein, we introduce 4-methoxyanilinium cation as a directed-pendulum unit to cause a polar structural phase transition. The methoxyl group looks like an ancient Chinese bola or a magnificent spider in natural kingdom and can be used as a directed pendulum or oscillator (Figure 1). The methyl terminal can undergo bola-like orientations and play a key role in the formation of molecular polarization. Such a polar solid pendulum-like phase may lead to molecular pendulum-like ferroelectrics, which, as we are aware, have never been found before.

2. EXPERIMENTAL SECTION

Synthesis. All reagents and solvents in the syntheses were of reagent grade and used without further purification. 4-Methoxyanilinium tetrafluoroborate-18-crown-6 (**1**) was prepared by slow evaporation of the

Received: May 18, 2011
Published: July 11, 2011

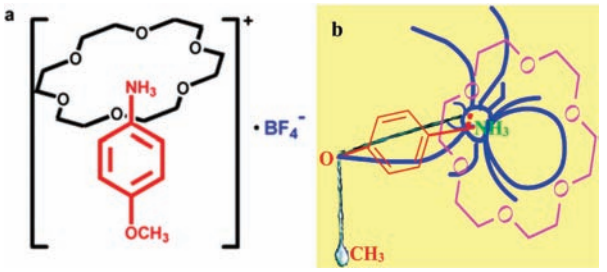

Figure 1. Schematic structure of **1**. (a) The basic unit of **1**. (b) The complex cation looks like an ancient Chinese bola or a magnificent spider.

solution (containing 1:1 of water and ethanol) under 4-methoxyanilinium tetrafluoroborate and 18-crown-6 in a 1:1 molar ratio. Colorless block crystals were obtained with a yield of about 40% based on 18-crown-6 after a few days. The phase purity is confirmed by its IR and XRD matching with its single crystal structural determination (see Supporting Information, Figures S1 and S2).

Measurement Methods. Infrared (IR) spectra were recorded on a Shimadzu IRPrestige-21. Powder X-ray diffraction (PXRD) was measured on a Rigaku D/MAX 2000 PC X-ray diffraction instrument. DSC measurements were performed on a PerkinElmer Diamond DSC under nitrogen atmosphere in aluminum crucibles with a heating or cooling rate of 10 K/min. Specific heat analyses were carried out on a Quantum Design PPMS. For dielectric measurements, the samples were made with the powder sample-pressed pellets. Silver conduction paste deposited on the surfaces was used as the electrodes. Complex dielectric permittivities were measured with an Agilent or a TH2828A impedance analyzer over the frequency range from 1 kHz to 1 MHz with an applied electric field of 0.5 V. For SHG experiments, an unexpanded laser beam with low divergence (pulsed Nd:YAG at a wavelength of 1064 nm, 5 ns pulse duration, 1.6 MW peak power, 10 Hz repetition rate) was used. The instrument model is FLS 920, Edinburgh Instruments and the low temperature system is 10−325 K, DE 202, while the laser is Vibrant 355 II, OPOTEK. The numerical values of the nonlinear optical coefficients for SHG have been determined by comparison with a KDP reference.

Single-Crystal X-ray Crystallography. X-ray diffraction experiments were carried out on **1** using a Rigaku Saturn 924 diffractometer with Mo Kα radiation (λ = 0.71073 Å) at various temperatures. Data collection, cell refinement, and data reduction were performed by using the CrystalClear software package (Rigaku). The structures of **1** were solved by direct methods and refined by the full-matrix method based on F^2 using the SHELXLTL software package. All non-hydrogen atoms were refined anisotropically, and the positions of all hydrogen atoms were generated geometrically. Crystal data for **1**: phase I (T = 93 K), $C_{19}H_{34}BF_4NO_7$, colorless block, 0.4 × 0.3 × 0.3 mm, M_r = 475.28, orthorhombic, $Pna2_1$, a = 15.913(3) Å, b = 12.505(3) Å, c = 11.285(2) Å, V = 2245.6(8) Å^3, Z = 4, D_{calc} = 1.406 g cm^{-3}, μ = 0.125 mm^{-1}, S = 1.041, $R(F)$ = 0.0324, w$R(F^2)$ = 0.0788; phase II (T = 243 K), orthorhombic, $Pnma$, a = 15.989(3) Å, b = 11.336(2) Å, c = 12.676(3) Å, V = 2297.6(8) Å^3, Z = 4, D_{calc} = 1.374 g cm^{-3}, μ = 0.122 mm^{-1}, S = 1.112, $R(F)$ = 0. 0485, w$R(F^2)$ = 0.1224.

3. RESULTS AND DISCUSSION

Crystal structural determination of **1** reveals the basic unit is composed of one $[C_7H_{10}NO(18\text{-crown-}6)]^+$ complex cation and one BF_4^- anion, and the protonated 4-methoxyanilinium cation joins with 18-crown-6 to form a rotator−stator assembly via N−H···O hydrogen-bonding interaction, as shown in Figure 2. At 93 K, the symmetry of the 18-crown-6 macrocycle

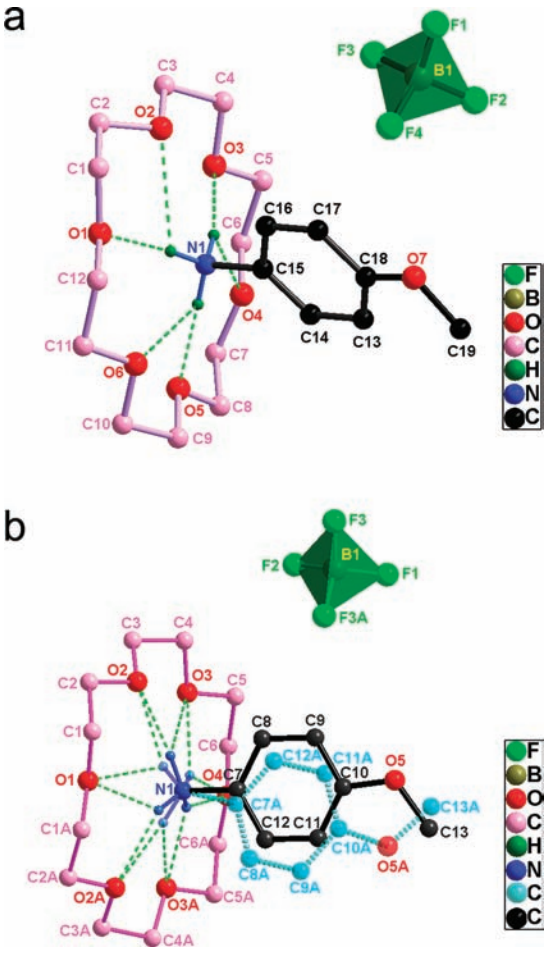

Figure 2. The asymmetric unit of **1** shown at different temperatures. (a) The low-temperature phase I (93 K): The 4-methoxyanilinium cation is totally ordered. (b) The close room temperature phase II (243 K): The 4-methoxyanilinium cation is totally disordered, not rotating within 360° but in the range of −30° to +30°, while the pendulum motion of methoxyl group is in the range of about −10° to +10° like a free pendulum (see the Supporting Information).

approximates to D_{3d}, corresponding to nearly ideal crown formation. The oxygen atoms of the 18-crown-6 in the structure are, as a common, displaced alternately above and below the median plane of the ring, forming two approximately parallel and nearly equilateral triangles. O1, O3, and O5 atoms are located above the mean O-atom plane (0.2446, 0.0795, and 0.2172 Å, respectively), and O2, O4, and O6 atoms are below the plane (0.1432, 0.1200 and 0.2781(18) Å, respectively). The N1 atom of the 4-methoxyanilinium cation is in the perching position, lying 0.7972(10) Å higher from the best plane of the oxygen atoms of the crown ring, rather than in the nesting position. The torsion angle between N1−C15 and the normal to the best plane is 8.2°. The intramolecular N−H···O hydrogen-bond distances are within the common range of 2.9761(18) and 2.8768(18) Å.

At close to room temperature, the asymmetric unit of **1** is halved as compared to that at 93 K, that is, one-half of the 18-crown-6 molecule, 4-methoxyanilinium cation, and BF_4^- anion. In the crystal, all three components lie on a common crystallographic mirror plane normal to [010]. The hydrogen-bonding interaction is strong between the 18-crown-6 molecule and 4-methoxyanilinium cation with the hydrogen bonds of N−H···O

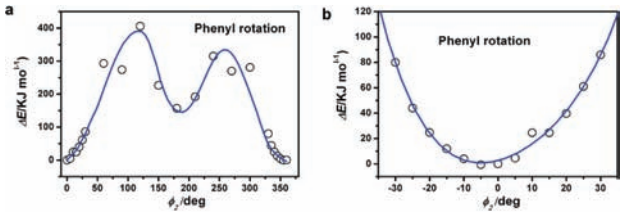

Figure 3. Potential energy curves for the pendulum motion of the phenyl ring along the C−O direction of the phenoxy group. (a) 360° rotation. (b) −30° to +30° pendulum motion.

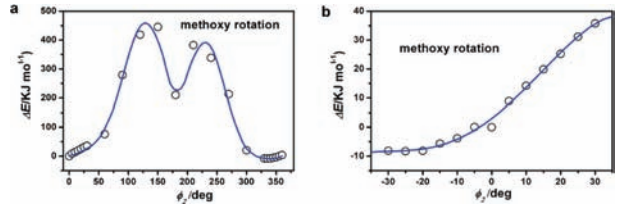

Figure 4. Potential energy curves for the pendulum motion of the methyl group along the C−O direction of the phenoxy group. (a) 360° rotation. (b) −30° to +30° pendulum motion.

ranging between 2.955(3) and 2.873(4) Å. The conformation of the macrocycle and the hydrogen-bond geometry in the complex cation closely resemble those in the low-temperature structure. The macrocycle adopts a conformation with an approximate D_{3d} symmetry, with all O−C−C−O torsion angles being gauche and alternating in sign and all C−O−C−C torsion angles being trans. The distances of the ether O atoms from their best plane are in the range between −0.0881 and 0.2727 Å. The C−N bond of the 4-methoxyanilinium cation is almost perpendicular to the mean plane of the crown-ether O atoms. The angle between N1−C7 and the normal to the best plane is 5.1°, which is slightly smaller than that in the low-temperature structure. The nitrogen of the $-NH_3^+$ group is also in the perching position, but a little higher from the plane of the oxygen atoms of the crown ring (0.8396 Å).

Because the changes of the order−disorder orientation of the phenyl ring and methoxyl group have been observed in the low and high temperature phases, we evaluated the potential energies of the rotation or motion of the phenyl ring and methoxyl group by using the RHF/6-31(d) basis set and the atomic coordinates at 93 K (Figures 3 and 4). When calculating the rotation angle dependence of the rotation of the phenyl ring along the C−C axis, the atomic coordinates of the $-NH_3^+$ and −OMe groups were fixed and a rigid rotation of the phenyl ring was applied. We evaluated the rigid rotation of the methoxyl group with the fixed atomic coordinates of anilinium moiety of *p*-methoxyanilinium. The nearest-neighboring two BF_4^- anions, three [18]-crown-6 ether, and two 4-methoxyanilinium cations were included in the calculations to evaluate the effects of steric hindrance on the rotations of the phenyl ring and methoxyl group. The initial atomic coordinates from the X-ray crystal structural analyses at 93 K corresponded to the first potential energy minimum at the $\varphi = 0°$, whose relative energy was defined as zero. Figure 3 shows the calculation results as a rotation energy curve from 0° to 360° with a 30° step. The nonsymmetrical double-minimum type potential energy curves were observed in rotation potential energies of the phenyl ring and methoxyl group, where the second energy minimum was observed at about 180°. The potential energy barriers of the phenyl group rotation were observed at φ_1 = 90 and 270° with ΔE of about 400 and 350 kJ mol^{-1}, respectively. The energy calculation results of the rotation of the methoxyl group show two peaks at φ_1 = 90 and 270° with ΔE of about 450 and 400 kJ mol^{-1}, respectively. Because the magnitude of the potential energy barrier of **1** is larger than the thermal energy $k_BT \approx 2.5$ kJ mol^{-1} (T = 297 K), the rotation of the phenyl ring and methoxyl group is almost impossible at around room temperature. Contrarily, the pendulum motions of the phenyl ring and methoxyl group easily occur. To certify the possibility of pendulum motions, we calculated the relative energy for every 5° forward−backward motion within the range of −30° to 30° (Figure 4). The parabolic potential energy profile was observed for the forward−backward motion of the methoxyl group. Because the potential energy ΔE is quite small, the pendulum motion of the phenyl ring and methoxyl group should be easily activated at 300 K. Such a motion was frozen during the structural phase transition at 126 K when lowering the temperature. The pendulum motions of the phenyl ring and methoxyl group, especially the methyl group, affect the structural phase transition (see Supporting Information Figure S3).

The crystal structure of **1** near room temperature (243 K) belongs to the orthorhombic crystal system with a centrosymmetric space group of *Pnma* and nonpolar point group D_{2h}, belonging to a paraelectric phase. The 4-methoxyphenyl group is totally disordered like a rotator unit, indicating it should be in a high symmetric and more disordered state. The dynamically reorientational disorder shows a glass transition upon cooling. The low-temperature structure confirms the change to a low symmetric and more ordered state below the phase transition temperature (T_c = 126 K). It is associated with the orientational freezing in of the molecular motions. When the temperature decreases to 93 K, the crystal structure of **1** still belongs to an orthorhombic crystal system but with a noncentrosymmetric space group $Pna2_1$ and a polar point group C_{2v}, belonging to a ferroelectric phase. As expected, the 4-methoxyanilinium cation becomes totally ordered in the solid state. In the cooling process, symmetry breaking occurs with an Aizu notation of *mmmFmm*2; that is, the eight symmetric elements (E, C_2, C_2', C_2'', i, σ_h, σ_v, σ_v) in the paraelectric phase (above 126 K) are halved into four (E, C_2, σ_v, σ_v) in the ferroelectric phase, reflecting a typical second-order feature according to Landau phase transition theory. This kind of ferroelectric phase transition is reminiscent of $(NH_4)_2SO_4$ and $(NH_4)_4BeF_4$, which undergo ferroelectric phase transitions from *Pnma* to $Pna2_1$. According to the Curie symmetry principle, the space group in the low-temperature phase is a subgroup of the one in the high-temperature phase (primary phase). In our case, $Pna2_1$ is a subgroup of *Pnma* whose maximal nonsubgroups include $Pna2_1$, $Pmn2_1$, $Pmc2_1$, $P2_12_12_1$, $P2_1/c$, and $P2_1/m$.

The space group change from *Pnma* (or $P\,2_1/n\,2_1/m\,2_1/a$) to $Pna2_1$ (or $P\ n\ 2_1\ a$) during the phase transition process is depicted in Figure 5. The mirror symmetry in [010] is broken. Thus, the 2-fold screw axis along the *a*- and *c*-axes and the inversion center disappear. The screw axis along the *b*-axis remains unchanged, leading to the final low-temperature space group $Pna2_1$. It is noted that the number of the symmetry operations in *Pnma* decreases by half from 8 to 4 in $Pna2_1$, in perfect agreement with the symmetry breaking analysis.

Furthermore, from the packing views along the *c*-axis, at paraelectric phase due to disordered character of phenyl ring and pendulum motion of methoxyl group, dipolar moment is canceled

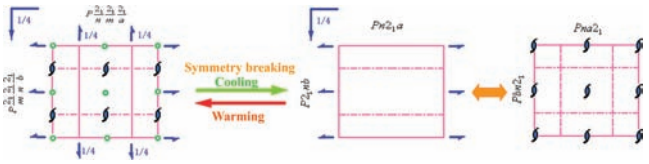

Figure 5. The transformation of space group of **1** from paraelectric phase (high-temperature phase) to ferroelectric phase (low-temperature phase). Symmetry operations for *Pnma*: (1) 1, (2) 2(0, 0, 1/2) 1/4, 0, *z*, (3) 2(0, 1/2, 0) 0, *y*, 0, (4) 2(1/2, 0, 0) *x*, 1/4, 1/4, (5) $\bar{1}$ 0, 0, 0, (6) *a x*, *y*, 1/4, (7) *m x*, 1/4, *z*, (8) *n*(0, 1/2, 1/2) 1/4, *y*, *z*. Symmetry operations for $Pna2_1$: (1) 1, (2) 2(0, 0, 1/2) 0, 0, *z*, (3) *a x*, 1/4, *z*, (4) *n*(0, 1/2, 1/2) 1/4, *y*, *z*.

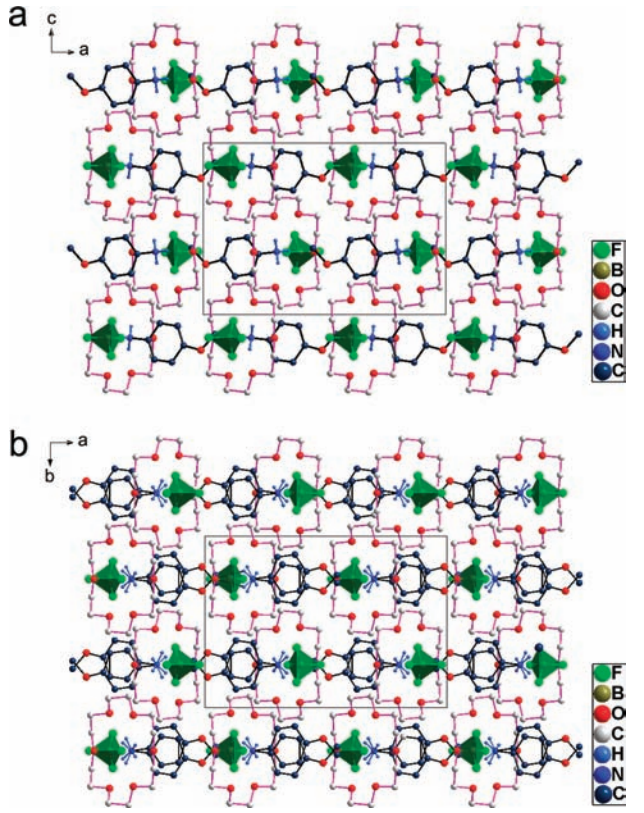

Figure 6. Packing views along the *c*-axis of the (a) ferroelectric and (b) paraelectric phases.

to display centrosymmetric packing status, while it is clearly seen that the 360° free rotation of the Ph−OMe part is completely impossible because the part is tightly sandwiched by 18C6 molecules and BF_4^- anions (Figure 6a), only making methoxyl group back and forth or pendulum motion within a small limited space (Figure 6b). Such, the polarization at 93 K (ferroelectric phase) lies in the fact that the methoxyl group is frozen to align in one direction so that the dipoles can not cancel each other along the *c*-direction due to the oriented arrangement of the dipoles of the cation, which is somewhat similar to that found in triglycine sulfate. This arrangement was broken by the pendulum motion of the Ph−OMe part in high temperature (paraelectric phase) due to molecular thermal motion (Figure 6b) supported by *c*-axis dielectric measurements mentioned below.

For a stress-free crystal, an analytical derived Gibbs free energy expression of the phase transition based on Landau theory is as

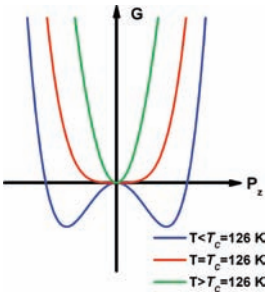

Figure 7. Gibbs free energy as a function of polarization P_z (order parameter) for the second-order phase transition of **1**. $T < T_c = 126$ K is for a stable ferroelectric phase (blue line), and $T > T_c = 126$ K is for a stable paraelectric phase (green line).

follows:

$$G = G_0 + \frac{1}{2}A(P_x^2 + P_y^2 + P_z^2) + \frac{1}{3}BP_xP_yP_z + \frac{1}{4}C(P_x^4 + P_y^4 + P_z^4) + \frac{1}{2}D(P_x^2P_y^2 + P_x^2P_z^2 + P_x^2P_z^2) + \frac{1}{3}E(P_x^3P_yP_z + P_y^3P_xP_z + P_z^3P_xP_y) + \frac{1}{6}F(P_x^6 + P_y^6 + P_z^6) + \frac{1}{4}H(P_x^4P_y^2 + P_x^4P_z^2 + P_y^4P_x^2 + P_y^4P_z^2 + P_z^4P_x^2 + P_z^4P_y^2) + \frac{1}{2}KP_x^2P_y^2P_z^2 + \ldots \quad (1)$$

where P_x, P_y, P_z are the polarization vectors of **P** along the three axial directions. From the Aizu expression of *mmmF*2 *mm*, it is known that the polar axis is along the *z* axis [001] and $P_x = P_y = 0$. Hence, the free energy expression (1) can be reduced to

$$G = G_0 + \frac{1}{2}AP_z^2 + \frac{1}{4}CP_z^4 + \frac{1}{6}FP_z^6 + \ldots \quad (2)$$

where *A* is linear relative to the temperature factor *T*, giving $A = \alpha_o(T - T_c)$, where T_c is the phase transition temperature. If assuming that the sign of the coefficient is positive, we can make diagrams of the Gibbs free energy *G* evolving with the variation of polarization P_z (Figure 7), noting that electric displacement $D = \varepsilon_o E + P$ and the paraelectric−ferroelectric phase transition happens at $T = T_c = 126$ K. As seen in Figure 7, if $T < T_c = 126$ K, there are two *G* minima corresponding to two equal and mutually inversed spontaneous polarizations, corresponding to the ferroelectric state, while if $T > T_c = 126$ K, *G* has only a minimum at $P_z = 0$, corresponding to the paraelectric state. On the other hand, noting that $\partial G/\partial P_z = E_z$, $\partial E_z/\partial P_z = \varepsilon^{-1}$, eq 2 can be rewritten as $\varepsilon^{-1} = a(T - T_c)$. It is the well-known Curie−Weiss law if ignoring the influence of the biasing electric field part $(+3CP_z^2 + 5FP_z^4 + \ldots)$.

DSC measurement clearly reveals that a phase transition occurred at about 126 K (Figure 8a). The entropy change (ΔS) accompanying the transition around $T_c = 127$ K is equal to about 2.79 J mol^{-1} K^{-1} ($\approx R$ ln 3/2), suggesting an "order−disorder" mechanism for this transition. From the shape of the observed anomalies, the value of the slight temperature hysteresis (~2 K), as well as the entropy change ΔS, it is obvious that this transition is a second-order transition. Specific heat capacity measurements were performed in the temperature range between 80 and 180 K (Figure 8b). The entropy change ΔS connected with the anomaly is estimated to be 2.71 J mol^{-1} K^{-1}. The characteristic anomaly is observed at 126 K, and the round

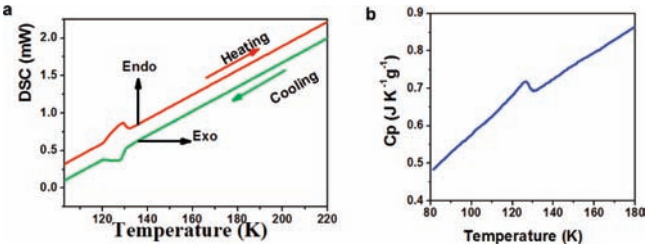

Figure 8. Thermal measurements of **1**. (a) DSC curves obtained on a heating−cooling cycle. (b) The temperature dependence of the heat capacity C_p.

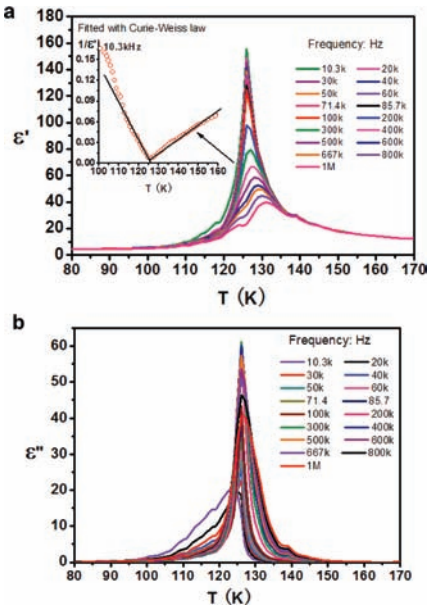

Figure 9. Temperature-dependent complex dielectric constant (ε) of **1** along the *c*-axis. (a) Real part of the complex dielectric constant at different frequencies. Inset plot is the reciprocal of the real part of the complex dielectric constant versus temperature. (b) Imaginary part of the complex dielectric constant at different frequencies.

shape of the anomaly peak most likely resembles the feature of a second-ordered phase transition.

Dielectric permittivity measurements of **1** are depicted in Figure 9, where the complex dielectric constant $\varepsilon = \varepsilon' - i\varepsilon''$, and ε' and ε'' are the real and imaginary parts of ε. At low frequencies, ε' reaches a maximum of about 160 at T_c, and its temperature dependence is typical of a continuous ferroelectric phase transition. To verify the continuous character of the phase transition, the temperature dependence of the reciprocal of ε' is plotted (Figure 9a). It is linear and does not reveal any discontinuities near the Curie point. According to the Curie−Weiss law, $\varepsilon = \varepsilon_\infty + C/(T - T_c)$, the fitted constant C_{para} of the paraelectric phase falls between 548 and 616 K at 10.3 kHz to 1 MHz, comparable to those found in colemanite, NH_4HSO_4, $[NH_2CH_2COOH]_2HNO_3$, and $(CH_3NH_3)Al(SO_4)_2 \cdot 12H_2O$ with values within 2×10^2 K, and the C_{ferro} of the ferroelectric phase falls between 196 and 154 K. These values are typical of the order−disorder-type ferroelectrics. The ratio of the Curie−Weiss constants C_{para}/C_{ferro} is 2.8−4.0, larger than 2 at low frequencies, and approximate to 4 at high frequencies as predicted theoretically for second-order phase transitions. It is similar to the

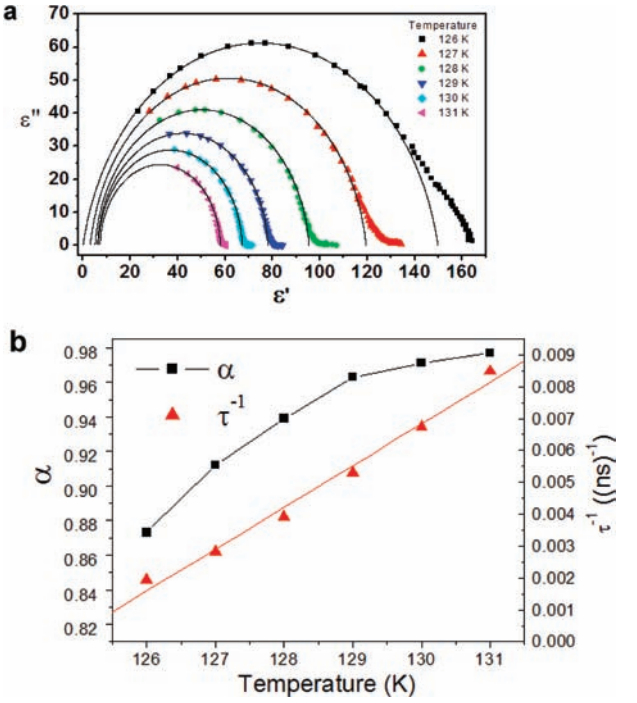

Figure 10. Relaxation behavior of **1**. (a) Cole−Cole diagrams in the paraelectric phase. The solid lines represent the fitting to the Debye-type relaxation mode. (b) Temperature dependence of α and τ^{-1}.

value of triglycine sulfate,[18] which is usually considered as a typical example of ferroelectrics with continuous phase transition. It is interesting to note that the ε' gradually exhibits two shoulder peaks when the frequency increases, in good agreement with that found in diglycine nitrate, which is a typical order−disorder-type ferroelectric showing relaxation character.

The temperature dependence of the dielectric permittivity of **1** discloses sharp maxima at the Curie point, and the values decrease with the increase of the measuring frequency. Such a temperature dependence of the complex permittivity is known as critical slowing down. Figure 10a shows the Cole−Cole plots in the paraelectric phase for a few temperatures close to the ferroelectric Curie point. In the paraelectric phase, the shape of the Cole−Cole plots suggests an almost monodispersive character of the complex permittivity whose frequency dependence can be described by eq 3:

$$\varepsilon = \varepsilon_\infty + \frac{\varepsilon_0 - \varepsilon_\infty}{1 + (i\omega\tau)^\alpha} \tag{3}$$

where ε_0 and ε_∞ are the static and high-frequency permittivities. The real and imaginary parts of the complex dielectric constant can be, respectively, written as:

$$\varepsilon' = \varepsilon_\infty + \frac{(\varepsilon_s - \varepsilon_\infty)\left(1 + \omega^\alpha\tau^\alpha \cos\frac{\alpha\pi}{2}\right)}{1 + 2\,\omega^\alpha\tau^\alpha \cos\frac{\alpha\pi}{2} + \omega^{2\alpha}\tau^{2\alpha}} \tag{3.1}$$

$$\varepsilon'' = \frac{(\varepsilon_s - \varepsilon_\infty)\,\omega^\alpha\tau^\alpha \sin\frac{\alpha\pi}{2}}{1 + 2\,\omega^\alpha\tau^\alpha \cos\frac{\alpha\pi}{2} + \omega^{2\alpha}\tau^{2\alpha}} \tag{3.2}$$

The fitted value of α is about 0.98 when $T - T_c$ equals 5 K and decreases with the decrease of temperature (Figure 10b). Near

dx.doi.org/10.1021/ja204540g |J. Am. Chem. Soc. 2011, 133, 12780–12786

the Curie point, α is 0.87, meaning an appearance of some polydispersity. In the ferroelectric phase, there are two relaxation processes (Figure 9b). One is related to the critical slowing and the other to dielectric dispersion due to the domain-wall motion.[19] The critical slowing is a result of the relaxation of fluctuation in the order parameter described by the Landau–Khalatnikov equation.[20] The relaxation time critically depends on the temperature:

$$\tau \approx (T - T_c)^{-1} \quad (4)$$

Equation 4 could be rewritten in a more convenient form:

$$\tau = \frac{\tau_0 T_c}{T - T_c} \quad (5)$$

where τ_0 is a relaxation time characteristic of the critical slowing. Figure 10b presents the temperature dependence of the inverse relaxation time τ^{-1}. Above the Curie temperature, τ^{-1} is well fitted with eq 4 with T_c value of 125.1 K, which is consistent with the phase transition temperature observed by DSC. The estimated characteristic time τ_0 of the paraelectric phase is 6.12 ns and is about 4 orders of magnitude longer than the relaxation times of hydrogen-bonded ferroelectrics.[21,22] This means that hydrogen bonds do not play an important role in the ferroelectric phase transition of **1** of which the estimated activity energy and relaxation time are about 59.28 kJ mol^{-1} and 1.50 × 10^{-30} s, respectively (see Supporting Information, Figures S4 and S5). Thus, the pendulum motion of the methoxyl group at paraelectric phase results in the dipolar moment cancellation so that above T_c there is no dielectric anomaly observed. At the same time, the frequency dependence of dielectric constant varies from 39 at 1 MHz to 158 at 5 kHz, suggesting that this motion should be evident at low frequency in good agreement with dipolar motion character. After cooling to T_c, this pendulum motion of methoxyl group is frozen to result in the creation of the dipolar moment so that ferroelectric phase is formed below T_c. The dielectric hysteresis loop measured at relatively low frequency supports the fact that the domain conversion correlates with the pendulum motion of methoxyl group only along the *c*-axis.

Dielectric hysteresis loops (D–E loops) on the *c* plane (001) of **1** are shown in Figure 11 at several temperatures. The maximum electric field E_{max} is about 11.4 kV cm^{-1}. On cooling from 146 K, the loop is initially a straight line, and no change occurs until around 127 K, showing **1** still in the paraelectric phase. Next, the line begins to open and suddenly grows into a typical ferroelectric loop at about 122 K, which is below the Curie temperature T_c, showing the current phase is ferroelectric. Upon further cooling, the ferroelectric loops completely open to reach saturation at about 109 K with a spontaneous polarization of about 0.54 μC cm^{-2} and a remanent polarization of 0.45 μC cm^{-2}, which is slightly larger than those found in Rochelle salt (0.2 μC cm^{-2}), lithium ammonium tartrate (0.20 μC cm^{-2}), guanidinium alumminium sulfate hexahydrate (0.35 μC cm^{-2}), ammonium sulfate (0.25 μC cm^{-2}), and dicalcium strontium propionate (0.30 μC cm^{-2}), and comparable to that of colemanite (0.65 μC cm^{-2}), but significantly smaller than that of triglycine sulfate (3.5 μC cm^{-2}). According to the Landau phase transition theory mentioned above, the saturation polarization (P_s) can be calculated by the phenomenological relation, $\Delta S = (2\pi/C)\cdot P_s^2$, holding for the second-order ferroelectric phase transition, where ΔS is the entropy change at T_c, C is the Curie–Weiss constant, and P_s is the spontaneous polarization in the vicinity of the Curie temperature. If putting ΔS = 2.79 J mol^{-1} K^{-1} and C = 241 K at 7 kHz into the equation, the calculated P_s is 0.59 μC cm^{-2}, in good agreement with the experimental result. When an external electric field applied, the Gibbs free energy should be written as:

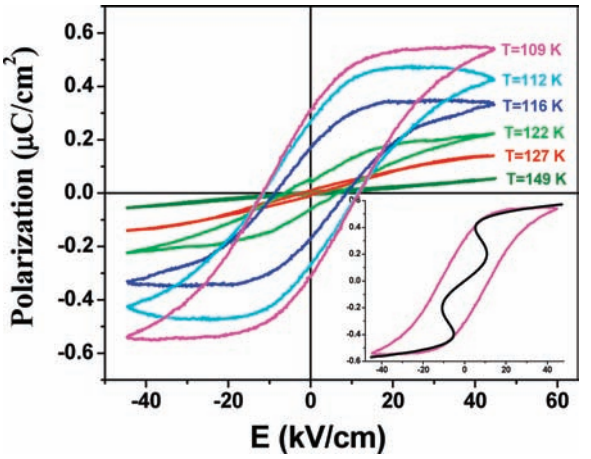

Figure 11. Dielectric hysteresis loops of **1** recorded along the *c*-axis. The measured frequency is fixed at about 50 Hz. The black line in the inset shows the fitting of hysteresis loop at 109 K using Landau theory.

$$G_1 = G_0 + \frac{1}{2}AP_z^2 + \frac{1}{4}CP_z^4 + \frac{1}{6}FP_z^6 - EP_z \quad (6)$$

where E is the applied electric field. Thus, the free energy reaches its extreme value when

$$\partial G_1/\partial P_z = AP_z + CP_z^3 + FP_z^5 - E = 0 \quad (7)$$

The fitted hysteresis loops are shown in the inset of Figure 11 by black solid lines. The fitted value of C is negative, which means a first-order phase transition. This suggests that this phase transition may be mixture-type, that is, contains both less partially first-order and more partially second-order character, which is similar to those found in $[Me_3NCH_2CO_2]CaCl_2\cdot 2H_2O$ and $[Me_4N]_2ZnI_4$ where they both display second-order with some first-order character.[23]

The electric-dipole contributions to second harmonic generation (SHG) have been studied in many piezoelectric and ferroelectric crystals, and the underlying microscopic mechanisms are well understood. According to the Gibbs free energy based on Landau theory (eq 2), dielectric constant can be deduced by the second-order differential of eq 2 with respect to electric displacement D as:

$$\frac{1}{\varepsilon} = \alpha + 3\beta D^2 + 5\gamma D^4 \quad (8)$$

where $D = D_E + P_s$ (D_E is the electric displacement induced by external electric field, and P_s is spontaneous polarization). The refractive index can be written as: $n^2 = \varepsilon_\infty/\varepsilon_0$. Therefore, eq 8 is reduced as:

$$\frac{1}{n^2} - \frac{1}{n_0^2} = (6\varepsilon_0\beta P_S + 20\varepsilon_0\gamma P_S^3 + \ldots)D_E + (3\varepsilon_0\beta + 30\varepsilon_0\gamma P_S^2 + \ldots)D_E^2 = \chi^{(2)}D_E + \chi^{(3)}D_E^2 \quad (9)$$

where n_0 is the refractive index without external electric field,

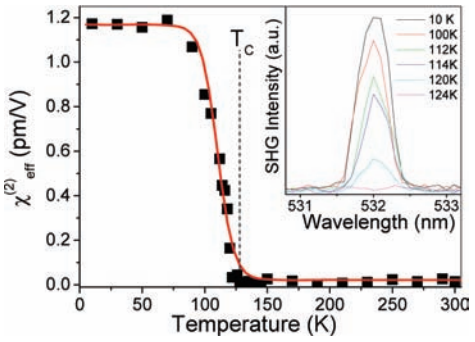

Figure 12. Temperature dependence of second-order nonlinear optical coefficient. The inset shows the SHG intensity as a function of wavelength at different temperatures. The sample particle size is about at 80−100 mesh (150−200 μm). Below 100 K, the intensity (measured at 10, 30, 50, 90 K) becomes almost saturated and does not increase any more. For clarity, only six curves were shown in the inset, and the detailed results were added in the Supporting Information.

$\chi^{(2)}D_E$, and $\chi^{(3)}D_E^2$ indicates the distortion of index ellipsoid induced by electric field. If we ignore high-order terms, we get $\chi^{(2)} = 6\varepsilon_0\beta P_s$ and $\chi^{(3)} = 3\varepsilon_0\beta$. Because β is almost independent of temperature, it is clearly shown that the behavior of temperature dependence of second-order nonlinear coefficient is consistent with that of spontaneous polarization. The temperature dependence of SHG is shown in Figure 12. Above 124 K, there is not any signal at 532 nm. However, below 124 K, a clear peak appears at 532 nm. It indicates that the structure of **1** turns from a centrosymmetric structure above 124 K to a noncentrosymmetric structure below 124 K, which is consistent with the XRD structure analysis (space group changes from *Pnma* to *Pna*2_1). It should be pointed out that the SHG effect is very sensitive to confirmation of noncentrosymmetric structure and has found a lot applications in inorganic oxide ferroelectrics, which is very useful for the confirmation of symmetry breaking and domain existence.[24] The second-order nonlinear coefficient $\chi^{(2)}$ is saturated with value of 1.17 pm/V below 70 K, which exceeds the value of KDP (about 0.9 pm/V). It hints that this sample may be one of the potential organic nonlinear optical (NLO) materials.

4. CONCLUSION

The present work has successfully demonstrated that the supramolecular assembly of crown ether cavity as guest-stator and guest molecule bearing a bola-like group plays an important role in the creation of supramolecular bola-like ferroelectrics, which is distinct from the precedent ferroelectrics. At the same time, the symmetry-breaking phase transition involves methyl group pendulum motions; that is, the freezing of pendulum motion at low temperature forces significant orientational motions of the guest molecules and thus induces the formation of the ferroelectric phase. This kind of bola-director-like group in molecular systems will open a new avenue for the design of polar functional materials.

■ ASSOCIATED CONTENT

Supporting Information. IR spectrum, powdered XRD patterns, calculated structures, complex permittivity at different frequencies, packing views, other mode calculations, SHG intensity, complete ref 24a, and X-ray crystallographic CIF file. This material is available free of charge via the Internet at http://pubs.acs.org.

■ AUTHOR INFORMATION

Corresponding Author
zhangwen@seu.edu.cn; xiongrg@seu.edu.cn

■ ACKNOWLEDGMENT

This work was supported by the National Natural Science Foundations of China [20931002, 90922005, and 21071030] and Jiangsu Province (BK2008029). R.-G.X. thanks the reviewers for excellent suggestions and Prof. T. Nakamura from Hokkaido University for potential energy calculations.

■ REFERENCES

(1) Scott, J. F.; Araujo, C. A. *Science* **1989**, *246*, 1400.
(2) Lee, H. N. H.; Christen, M.; Chrisholm, M. F.; Rouleau, C. M.; Lowndes, D. H. *Nature* **2005**, *433*, 395.
(3) O'Brien, Z. J.; Karlen, S. D.; Khan, S.; Garcia-Garibay, M. A. *J. Org. Chem.* **2010**, *75*, 2482.
(4) Gould, S. L.; Tranchemontagne, D.; Yaghi, O. M.; Garcia-Garibay, M. A. *J. Am. Chem. Soc.* **2008**, *130*, 3246.
(5) Dominguez, Z.; Khuong, T.-A. V.; Dang, H.; Sanrame, C. N.; Nuñez, J. E.; Garcia-Garibay, M. A. *J. Am. Chem. Soc.* **2003**, *125*, 8827.
(6) Karlen, S. D.; Reyes, H.; Taylor, R. E.; Khan, S. I.; Hawthorne, M. F.; Garcia-Garibay, M. A. *Proc. Natl. Acad. Sci. U.S.A.* **2010**, *107*, 14973.
(7) Garcia-Garibay, M. A. *Proc. Natl. Acad. Sci. U.S.A.* **2005**, *102*, 10771.
(8) Vacek, J.; Michl, J. *Proc. Natl. Acad. Sci. U.S.A.* **2001**, *98*, 5481.
(9) Akutagawa, T.; Koshinak, H.; Sato, D.; Takeda, S.; Noro, S.; Takahashi, H.; Kumai, R.; Tokura, Y.; Nakamura, T. *Nat. Mater.* **2009**, *8*, 342.
(10) Akutagawa, T.; Koshinaka, H.; Ye, Q.; Noro, S.; Kawamata, J.; Yamaki, H.; Nakamura, T. *Chem. Asian J.* **2010**, *5*, 520.
(11) Zhang, W.; Cai, Y.; Xiong, R. G.; Yoshikawa, H.; Awaga, K. *Angew. Chem., Int. Ed.* **2010**, *49*, 6608.
(12) Zhang, W.; Ye, H. Y.; Cai, H. L.; Ge, J. Z.; Xiong, R. G.; Huang, S. P. D. *J. Am. Chem. Soc.* **2010**, *132*, 7300.
(13) Zhang, W.; Ye, H. Y.; Xiong, R.-G. *Coord. Chem. Rev.* **2009**, *253*, 2980.
(14) Zhang, W.; Chen, L. Z.; Xiong, R. G.; Nakamura, T.; Huang, S. P. D. *J. Am. Chem. Soc.* **2009**, *131*, 12544.
(15) Ye, H. Y.; Fu, D. W.; Zhang, Y.; Zhang, W.; Xiong, R.-G.; Huang, S. P. D. *J. Am. Chem. Soc.* **2009**, *131*, 42.
(16) Zhang, W.; Xiong, R. G.; Huang, S. P. D. *J. Am. Chem. Soc.* **2008**, *130*, 10468.
(17) Ye, Q.; Song, Y. M.; Wang, G. X.; Chen, K.; Fu, D. W.; Chan, P. W. H.; Zhu, J. S.; Huang, S. P. D.; Xiong, R. G. *J. Am. Chem. Soc.* **2006**, *128*, 6554.
(18) Hoshino, S.; Mitsui, T.; Jona, F.; Pepinsky, R. *Phys. Rev.* **1957**, *107*, 1255.
(19) Shin, Y.-H.; Grinberg, I.; Chen, I.-W.; Rappe, A. M. *Nature* **2007**, *449*, 881.
(20) Patashinskii, A. Z.; Pokrovskii, V. L. *Fluctuation Theory of Phase Transitions*; Pergamon Press: Elmsford, NY, 1979.
(21) Szafrański, M.; Katrusiak, A.; McIntyre, G. J. *Phys. Rev. Lett.* **2002**, *89*, 215507.
(22) Horiuchi, S.; Tokura, Y. *Nat. Mater.* **2008**, *7*, 357.
(23) Hang, T.; Zhang, W.; Ye, H.-Y.; Xiong, R.-G. *Chem. Soc. Rev.* **2011**, *40*, 3577.
(24) (a) Lee, J. H.; et al. *Nature* **2010**, *469*, 954. (b) Neacsu, C. C.; van Aken, B. B.; Fiebig, M.; Raschke, M. B. *Phys. Rev. B* **2009**, *79*, 100107(R).